Pol. J. Environ. Stud. Vol. 31, No. 5 (2022), 4767-4777
DOI: *10.15244/pjoes/150460* ONLINE PUBLICATION DATE: 2022-09-13

Original Research

Surface Ozone in the Central Plains Urban Agglomeration, China: Spatial-Temporal Variations and Health Impacts

Xiaoyong Liu[1, 2], Jiqiang Niu[1, 2]*, Jun Yan[1, 2], Junhui Yan[1, 2], Chengmei Zhao[1, 2], Feng Xu[1, 2], Yidan Zhang[1, 2], Bingbing Zhang[1, 2]

[1]School of Geographic Sciences, Xinyang Normal University, Xinyang 464000, China
[2]Henan Key Laboratory for Synergistic Prevention of Water and Soil Environmental Pollution, Xinyang Normal University, Xinyang 464000, China

Received: 27 April 2022
Accepted: 26 May 2022

Abstract

To investigate the spatial-temporal variations and health impacts of O_3 (ozone) in the Central Plains Urban Agglomeration, China (CP-UA), multiple and transdisciplinary methods were employed to analyze the collected millions of O_3 concentrations data. The results showed that the annual average concentration of O_3 in the CP-UA reduced by 19.7% from 2017 to 2020. O_3 monthly concentrations exhibited a multimodal structure and a feature of "high in summer and winter, low in spring and autumn". In spatial distribution, the main distribution of O_3 concentration was aligned in the northwest-southeast direction in the CP-UA. O_3 concentrations displayed positive spatial autocorrelations. The most polluted cities were distributed in northern CP-UA, forming a high-high (HH) agglomeration of O_3 concentrations. Cities in southern CP-UA had low O_3 concentrations, forming a low–low (LL) agglomeration pattern. It was estimated that the premature mortalities attributed to O_3 for respiratory disease in warm months were 15, 960 per year. The premature mortalities decreased by 28.7% in 2020 compared to 2017. The rescaled range analysis suggested a declining trend of O_3 concentrations and premature mortalities in the CP-UA.

Keywords: ozone, central plains urban agglomeration, spatial-temporal variations, health impacts

Introduction

With the rapid economic development, industrial expansion, and urbanization over the past decades, China has experienced serious O_3 (ozone) pollution, which has attracted much attention from the public, government, and researchers [1-4]. O_3 is secondary air pollution attributed to the photochemical reactions between nitrogen oxides (NO_x) and volatile organic compounds (VOCs) under solar radiation [3]. Motor vehicles and industrial activities are the main sources of O_3 precursors [5]. High concentrations of ozone can cause heavy smog in metropolitan cities, harm human health, and affect crop yield [6, 7]. From 2013 to 2016, surface O_3 concentrations have increased by

*e-mail: niujiqiang@xynu.edu.cn

10.8% in China [8]. The increasing O_3 concentrations caused hundreds of thousands of premature mortalities [9], millions of metric tons of losses of key crops [6], and billions of dollars in economic losses [10]. O_3 has become the second most important air pollutant after $PM_{2.5}$ in most cities of China.

Recently, extensive studies focused on urban agglomerations in China such as Beijing-Tianjin-Hebei (BTH), Yangtze River Delta (YRD), and Pearl River Delta (PRD) [10-14], to clarify the ozone spatiotemporal variations, regional transportations, and health impacts. The results demonstrated that the surface O_3 concentrations in megacities of China (e.g. Beijing, Shanghai, and Shenzhen) were much higher than the World Health Organization Standard (maximum daily 8-h average (MDA8) O_3>50 ppbv). As production of photochemical reactions, O_3 formation regimes relating to weather conditions, terrain, and precursors [16], leads to the different spatiotemporal patterns of O_3 among urban agglomerations. To our best knowledge, only a few studies focused on the regional O_3 pollution in the Central Plains Urban Agglomeration (CP-UA). CP-UA is the largest urban agglomeration in Central China, including 30 prefecture-level cities with a population of more than 160 million. CP-UA is seriously constrained by resources, and population agglomeration [17], causing high levels of $PM_{2.5}$ and O_3 [18]. All cities in Henan Province belong to the CP-UA. Zhengzhou, the capital city of Henan province and the regional central city of the CP-UA as well, was seriously O_3 polluted [19, 20], increasing the mortality risk of cardiovascular and respiratory [21]. Other cities in the CP-UA, e.g. Xingtai, Handan, Anyang, Jiaozuo, Pingdingshan, Liaocheng, and Yuncheng were characterized by industry or energy-consuming, which emitted a large amount of O_3 precursors and suffered serious O_3 pollution. Previous studies found that in Henan Province, due to O_3 pollution, the annual mean relative yield loss of wheat was 8.8%-14.1% [22], and the premature mortalities caused were about 7000 [23]. Therefore, deep and comprehensive research on surface O_3 in the CP-UA is necessary.

The present study aims to investigate the spatial-temporal variations and health impacts of ozone in the CP-UA by using multiple and transdisciplinary methods. Specifically, we (1) systematically characterize the annual, seasonal, monthly, and diurnal variations of ozone concentrations, (2) analyze the spatial patterns and variations of ozone, and (3) estimate the premature mortality attributed to O_3 exposure. Our findings are conducive to improving the understanding of the spatial-temporal patterns and the mechanisms of O_3 pollution in the CP-UA. Meanwhile, the findings provide scientific support for determining the efficient approach for O_3 reduction in CP-UA.

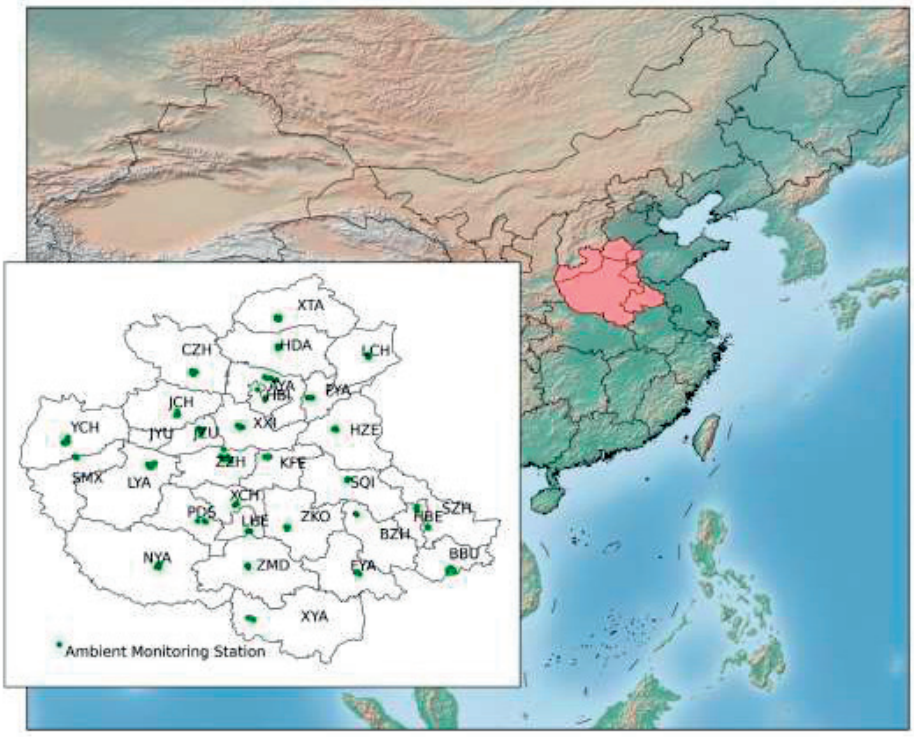

Fig. 1. Location and included cities of the Central Plains Urban Agglomeration (CP-UA) in China (AYA: Anyang, BBU: Bengbu, BZH: Bozhou, CZH: Changzhi, FYA: Fuyang, HBE: Huaibei, HBI: Hebi, HDA: Handan, HZE: Heze, JCH: Jincheng, JYU: Jiyuan, JZU: Jiaozuo, KFE: Kaifeng, LCH: Liaocheng, LHE: Luohe, LYA: Luoyang, NYA: Nanyang, PDS: Pingdingshan, PYA: Puyang, SMX: Sanmenxia, SQI: Shangqiu, SZH: Suzhou, XCH: Xuchang, XTA: Xingtai, XXI: Xinxiang, XYA: Xinyang, YCH: Yuncheng, ZKO: Zhoukou, ZMD: Zhumadian, ZZH: Zhengzhou). The blue dots represent O_3 monitoring sites.

Materials and Methods

Study Area

The CP-UA (31.4°N-37.8°N, 110.2°E-118.2°E) is located in central China (Fig. 1), including 30 cities: all 18 cities in Henan Province, Changzhi, Jincheng, and Yuncheng in Shanxi Province; Liaocheng and Heze in Shandong Province; Huaibei, Bengbu, Suzhou, Fuyang, and Bozhou in Anhui Province; and Xingtai and Handan in Hebei Province [24]. The CP-UA covers 287,000 km^2 with a population of more than 160 million.

Materials

A long time series of hourly concentrations of O_3 from January 2017 to December 2020 in the CP-UA were obtained from the national air quality monitoring network operated by China National Environmental Monitoring Center. Due to the absence of air quality monitoring site in Jiyuan, O_3 data was lacking. O_3 concentration was measured by Ultraviolet photometer or Differential Optical Absorption Spectroscopy. The instrumental operation, maintenance, and quality assurance/quality control are conducted according to the China Environmental Protection Standards "HJ 818-2018". We used O_3 daily maximum 8-hour sliding average (MDA8-O_3) concentration as the O_3 level of that day and used the 90th percentile of MDA8-O_3 as the annual assessment standard [25]. In this study, the seasonal, monthly (spring: March to May, summer: June to August, autumn: September to November, winter: January, February, and December), and daily variations of O_3 were calculated using the mean of the MDA8-O_3 in each city. The diurnal variations of O_3 concentrations were calculated using the hourly O_3 concentration of each city.

Methods

Kernel Density Estimation

Kernel density estimation was employed to calculate the O_3 density function, which is defined as:

$$f(x) = \frac{1}{nh}\sum_{i=1}^{n} K\left(\frac{x_i - x}{h}\right) \quad (1)$$

where n is the number of samples, h indicates the bandwidth, and K represents the kernel weighting function. In the present study, the Epanechnikov kernel and Silverman's bandwidth were used [26].

Standard Deviational Ellipse

The standard deviation ellipse (SDE), namely directional distribution [27], demonstrates elements in the main distribution area through four key parameters, i.e., center point, major axis, minor axis, and azimuth. The mean center is the central location for the entire dataset. The major and minor axes of the ellipse suggest the direction and range of the data distribution, respectively [28]. Azimuth defines the main trend direction. In this paper, the spatial feature of ozone in the CP-UA was identified by SDE. The main parameters of SDE are calculated as follows:

Mean Center:

$$x_{mc} = \frac{\sum_{i=1}^{n} w_i x_i}{\sum_{i=1}^{n} w_i} \quad (2)$$

$$y_{mc} = \frac{\sum_{i=1}^{n} w_i y_i}{\sum_{i=1}^{n} w_i} \quad (3)$$

where x_i and y_i are the coordinates for i, w_i represents the weight value, and n is equal to the total number of sites.

The angle of rotation is calculated as:

$$\tan\theta = \frac{A+B}{C} \quad (4)$$

$$A = \left(\sum_{i=1}^{n} \bar{x}_i^2 - \sum_{i=1}^{n} \bar{y}_i^2\right) \quad (5)$$

$$B = \sqrt{\left(\sum_{i=1}^{n} \bar{x}_i^2 - \sum_{i=1}^{n} \bar{y}_i^2\right)^2 + 4\left(\sum_{i=1}^{n} \bar{x}_i \bar{y}_i\right)^2} \quad (6)$$

$$C = 2\sum_{i=1}^{n} \bar{x}_i \bar{y}_i \quad (7)$$

where, $\bar{x}_i$ and $\bar{y}_i$ indicate the deviation of the xy-coordinates from the Mean Center.

The standard deviations for the x-axis and y-axis are:

$$\sigma_x = \sqrt{\frac{\sum_{i=1}^{n} (\bar{x}_i \cos\theta - \bar{y}_i \sin\theta)^2}{n}} \quad (8)$$

$$\sigma_y = \sqrt{\frac{\sum_{i=1}^{n} (\bar{x}_i sin\theta - \bar{y}_i cos\theta)^2}{n}} \quad (9)$$

Rescaled Range (R/S) Analysis

In this paper, the R/S analysis was employed to discuss the changing trend of O_3 concentration. The R/S analysis proposed by Hurst [29], is the ratio between range and standard deviation, which is calculated as follows [30]:

$$\overline{x} = \frac{\sum_{i=1}^{j} x_i}{j},\ j = 1, 2, 3, \ldots \quad (10)$$

$$x(i,j) = \sum_{k=1}^{i} x(k) - \overline{x}(j),\ 1 \le i \le j \quad (11)$$

$$R(j) = \max_{1\le i\le j} x(i,j) - \min_{1\le i\le j} x(i,j),\ j = 1, 2, 3, \ldots \quad (12)$$

$$S(j) = \left[\frac{1}{j}\sum_{i=1}^{j}(x(i) - \overline{x}(j))^2\right]^{\frac{1}{2}}, \quad j = 1, 2, 3, \ldots \quad (13)$$

where *x(i)*, *x(i,j)*, *R(j)*, and *S(j)* are the mean, cumulative dispersion, range, and standard deviation of the given time series, respectively. If x_i is a random sequence, then:

$$\frac{R(j)}{S(j)} = \left(\frac{\pi j}{2}\right)^H \quad (14)$$

where *H* indicates the Hurst index of the time series.

The *H* value ranges from 0 to 1. If *H* = 0.5, it indicates that the O_3 time series is random and there is no long-term relationship; If 0.5<H<1, it suggests that the O_3 time series has long-term persistence. The change in O_3 concentration in the future is consistent with the change trend in the past. The closer *H* is to 1, the stronger the persistence; If 0<H<0.5, it represents the O_3 time series is anti-sustainability. The change in O_3 concentration in the future is opposite to the change trend in the past. The closer *H* is to 0, the stronger the anti- sustainability.

Global and Local Spatial Autocorrelation Analysis

The spatial distributions of O_3 concentrations are related to spatiotemporal and geospatial processes. Therefore, the global Moran's I index was employed to quantitatively determine the global autocorrelation of O_3 in the CPUA. Detailed descriptions for the global Moran's I can be found in previous studies [31, 32]. The global Moran's I ranges from 0 to 1. A negative (positive) index suggests a negative (positive) correlation and the smaller (greater) the index, the stronger the spatial dispersion (agglomeration) of the O_3, while an I_{Global} of 0 indicates no spatial autocorrelation.

Global spatial autocorrelation can only judge whether the geographical variables have spatial autocorrelation but cannot reflect the characteristics of an urban spatial agglomeration within a region [17]. Therefore, the local Moran's I index was used to identify the distribution and agglomeration patterns of O_3 in the CPUA. Based on the calculated local Moran's I index, the spatial association modes can be classified into four types [33]: high-high clustering type (hereinafter HH), low-low clustering type (LL), low-high clustering type (LH), and high-low clustering type (HL). The index that fails the significance test is classified as not significant.

Human Health Impacts

High O_3 concentration can cause respiratory diseases, and the premature mortality attributed to O_3 exposure is estimated as formulas [34]:

$$\Delta M = y_o N(RR - 1)/RR \quad (15)$$

where ΔM represents the excess mortalities attributable to O_3 exposure, y_o is the baseline mortality rate, *N* indicates the exposed population, and *RR* is the relative risk. *RR* is calculated by:

$$RR = \exp\left(\beta(C - C_o)\right) \quad (16)$$

where β denotes the concentration-response coefficient, *C* and C_0 represent O_3 concentration and reference concentration, respectively.

In this study, the population data are from the seventh population census of China. The mortality rate for respiratory disease during 2017-2020 is collected from China Statistical Yearbook issues 2018, 2019, 2020, and 2021 (http://www.stats.gov.cn/tjsj/ndsj/), which is 67.2, 68.02, 65.02, and 55.36, respectively. The *RR* is 1.04, a 20 μg/m^3 increase in MDA8-O_3 concentration is associated with a 4% increase in *RR* of death from respiratory disease, and the recommended value of C_0 is 75.2 μg/m^3 [34].

Results and Discussion

Temporal Variations in O_3 in the Central Plains Urban Agglomeration

Annual Variation

Fig. 2 shows the estimated kernel density and over-standard rates of the O_3 concentrations in the CP-UA from 2017 to 2020. Overall, the annual average concentration of O_3 (90th percentile of MDA8-O_3) in the CP-UA was gradually reduced from 2017. Specifically, in 2020 the yearly average O_3 concentration amounted to 203.6 μg/m^3, and was reduced by 19.7% relative to that in 2017 (253.6 μg/m^3). As displayed in Fig. 2a), the peak of the kernel-density curves became steeper and moved to the left from 2017 to 2020, which indicated that O_3 concentrations in most of the cities of the CP-UA were continuously reduced. The upper tail of the density curves decreased over time, suggesting that cities with high O_3 concentrations (more than 250 μg/m^3), had substantial decrease in O_3 concentration. In 2017 the number of cities with annual O_3 concentrations greater than 220 μg/m^3 was 24, while the number decreased to 2 in 2020. As shown in Fig. 2b), the proportion of MAD8-O_3 exceeded the China National Ambient Air Quality Standards I (CAAQS grade I; 100 μg/m^3) in CP-UA over 2017-2020 was 81.6%. And the proportions exceeded the Grade 2 limit (160 μg/m^3) was 39.3%, indicating severe O_3 pollution. The proportion that exceeded the Grade 2 limit during 2017-2020 was 44.3%, 42.5%, 41.0%, and 29.3%, respectively, suggesting the reduction of O_3 pollution in the CP-UA. In other urban agglomerations of China, e.g., BTH, PRD, and YRD, O_3 concentrations also decreased from 2017 to 2020 [35], which indicated the Air Pollution Prevention

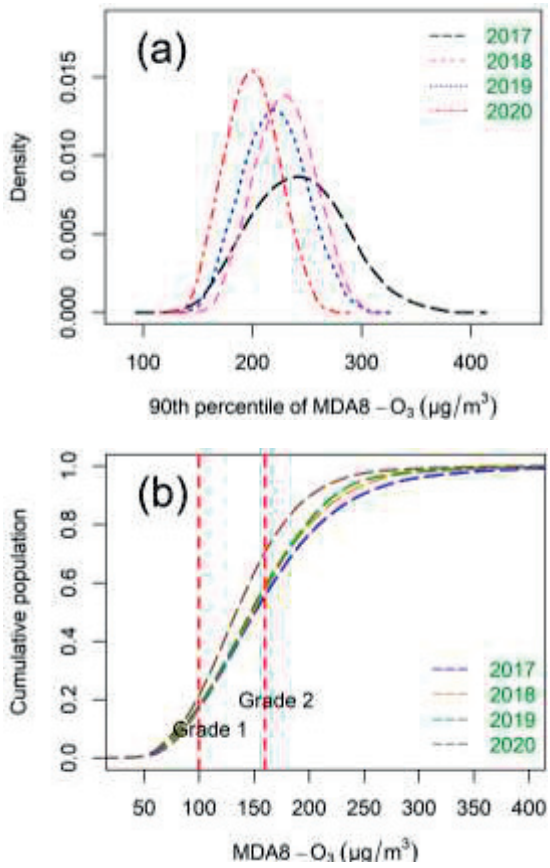

Fig. 2. a) Kernel-density estimates of annual mean O_3 concentrations and b) the annual over-standard rate of the O_3 concentrations in the CP-UA in 2017-2020.

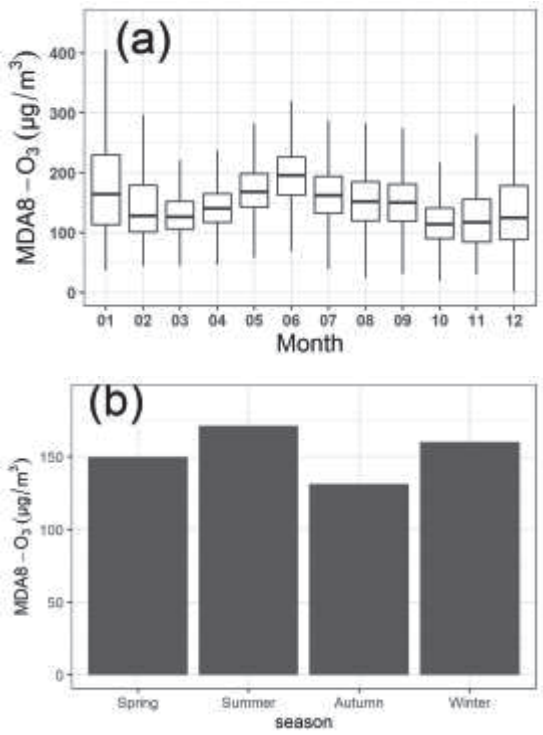

Fig. 3. a) Monthly and b) seasonal variation of MDA8-O_3 in the CP-UA over 2017-2020. Shown are the median (central horizontal bar within the boxes), 25th and 75th percentiles (lower and upper bars of the boxes, respectively), and minimum and maximum (lower and upper whiskers, respectively).

and Control Action Plan formulated by China government worked as intended.

Monthly Variation

The monthly characteristics of O_3 concentrations in the CP-UA over 2017-2020 are illustrated in Fig. 3a). Previous studies have pointed out that monthly variation characteristics in O_3 are related to latitude in China. The unimodal structure is generally found for latitudes over 35°N, whereas the bimodal structure is in most of the cases identified south of 35°N [36]. CP-UA covers a latitude of 31.4°N-37.8°N. A multimodal structure of O_3 monthly variation was found in CP-UA in this study. The monthly average O_3 concentrations showed an increasing trend from February to June, a decreasing trend from July to October, and an increasing trend in November and December. The highest monthly average concentrations occurred in June, with 195.5 μg/m^3. As displayed in Fig. 3b), the seasonal averages of the O_3 concentrations in the CP-UA during 2017-2020 in spring, summer, autumn, and winter were 149.8, 171.2, 131.1, and 160.0 μg/m^3, respectively. The O_3 concentrations showed a feature of "high in summer and winter, low in spring and autumn" in the CP-UA, which is different from the feature of "high in spring and summer, low in autumn and winter" in the YRD [35]. The meteorological conditions are the important factor that influences the monthly variation of O_3 in the CP-UA. In summer, the relatively high temperature and strong radiation enhance the photochemical reactions, which leads to increased O_3 production. In winter, most regions in China have the lowest O_3 levels [35, 36], while a high O_3 concentration was observed in the CP-UA in this study. An increasing winter-spring O_3 and increasing association of high ozone with winter haze events were found in the North China Plain [39]. We inferred that the high-level O_3 in winter in the CP-UA may be related to $PM_{2.5}$ concentration. The collaborative governance of $PM_{2.5}$ and O_3 become an important issue in the CP-UA.

Diurnal Variation

As the photochemical reactions product, O_3 concentrations are closely related to solar radiation. As shown in Fig. 4, The diurnal variation of O_3 concentrations exhibited a unimodal character in the CP-UA, with high O_3 concentrations in the daytime and low in the nighttime, which is consistent with other regions of China [40]. In the daytime, with the sun rising and solar radiation enhanced, anthropogenic precursors such as VOCs and NO_x participate in photochemical reactions and promote the formation of O_3 [41].

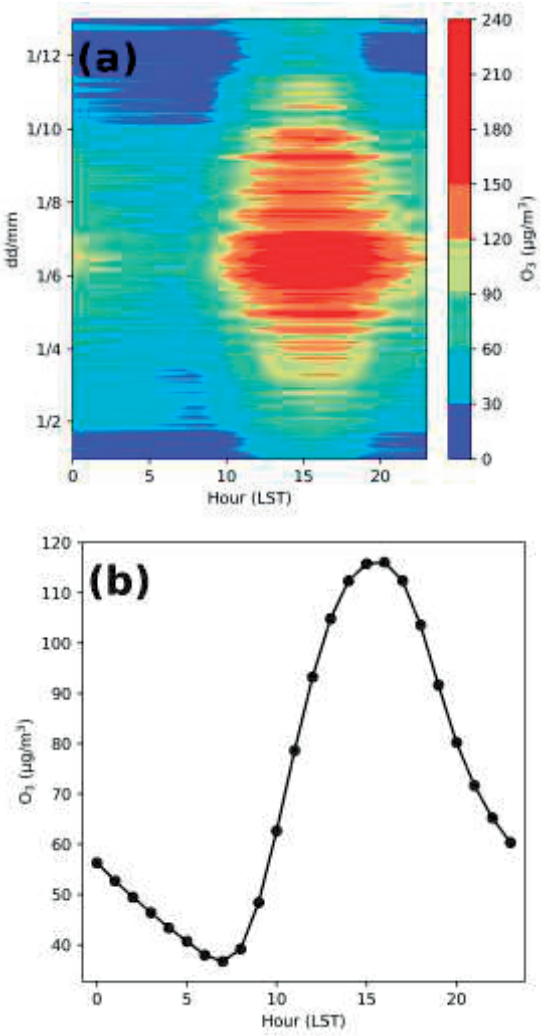

Fig. 4. Diurnal variations of O_3 concentrations in the CP-UA during 2017-2020.

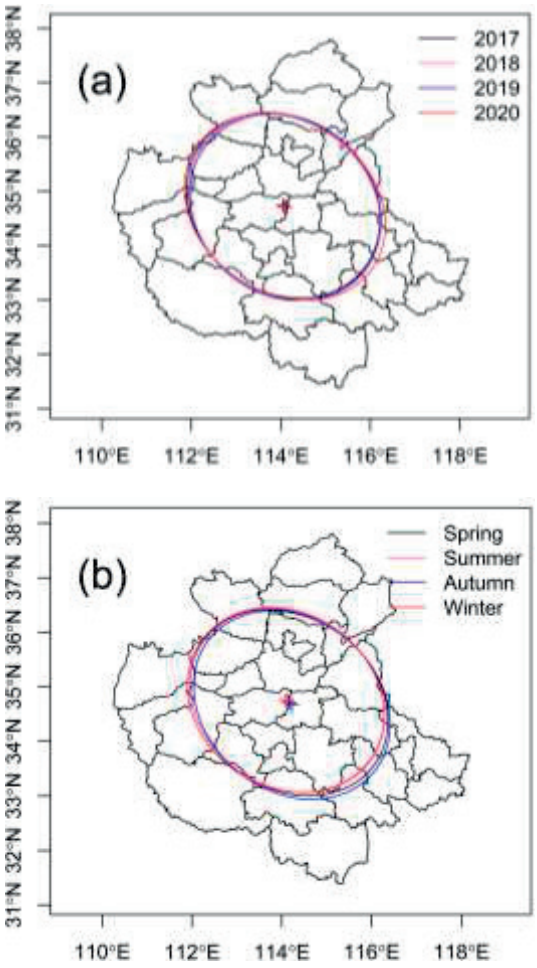

Fig. 5. Standard ellipse deviation distribution in a) different years and b) different seasons in the CP-UA.

The O_3 concentration increased during 8:00~16:00 (LST) and reached a maximum value of 116.1 μg/m^3 at 16:00 (Fig. 4b). Then the O_3 concentration decreased continually. During the night time, O_3 can be eliminated by NO_x titration reactions. Recent studies suggested that particulate matter can also react with O_3 and eliminate it from the atmosphere [42]. In June and July, the O_3 concentration was still high at 20:00 (Fig. 4a). O_3 concentration above 150 μg/m^3 lasted about 10 hours each day in June.

Spatial Distributions in O_3 in Central Plains Urban Agglomeration

Standard Deviational Ellipse Analysis

The overall variations in the spatial pattern of O_3 in the CP-UA in different years and seasons were characterized by SDE analysis. As displayed in Fig. 5a), the main distribution of O_3 concentration was aligned in the northwest-southeast direction in the CP-UA. The azimuth of the ellipse decreased from 123.2° in 2017 to 120.5° in 2020 (Table 1), which suggested the ellipse moved northward. The mean centers detected by SDE were located in northeastern Zhengzhou. From 2017 to 2020, the center of O_3 concentration across the CP-UA moved from 34.75°N, 114.05°E to 34.72°N, 114.09°E, which indicated a greater O_3 concentration decrease in northwestern CP-UA. The major axes of the ellipses increased from 211.6 to 220.5 km. The increase of the major axes illustrated the spatial aggregation tendency and the spatial changes in O_3 concentration from 2017 to 2020. The ratio between the major and minor axes of the ellipses presented an increasing tendency from 2017 to 2020, indicating the enhanced trend of directional distribution. As displayed in Fig. 5b), the seasonal variation of the standard deviation ellipse was more obvious than the annual variation. In summer and winter, the mean centers were located in Zhengzhou, and in spring and winter, the mean centers moved to Kaifeng. In winter, the major axes were the shortest (211.9 km) and the minor axes were the longest (176.3 km) in four seasons, and the ratio between the major and minor axes was lowest than in other seasons. This suggested that spatial dispersion of O_3

Table 1. Parameters of standard deviation ellipse in the Central Plains Urban Agglomeration.

Items	Variables	Parameters				
		Azimuth/degree	Mean center	Major axes/km	Minor axes/km	Area/km^2
Year	2017	123.20	114.05°E, 34.75°N	211.6	176.3	117189
	2018	125.41	114.08°E, 34.72°N	211.3	175.8	116702
	2019	125.19	114.10°E, 34.72°N	207.9	179.1	117017
	2020	120.53	114.09°E, 34.72°N	220.5	176.1	121953
Season	Spring	121.39	114.16°E, 34.71°N	217.0	174.6	119008
	Summer	121.96	114.12°E, 34.76°N	212.4	175.4	117026
	Autumn	124.15	114.22°E, 34.67°N	217.2	175.1	119483
	Winter	118.81	114.09°E, 34.75°N	211.9	176.3	117404

concentrations in the CP-UA was relatively strong in winter. In autumn, the directional distribution of O_3 concentrations was stronger than in other seasons. In summer, the area covered by the ellipse was the smallest (117026 km^2), accounting for 58.4% of the CP-UA.

Spatial Autocorrelation of O_3 Concentrations

The global Moran's I under different years and seasons in the CP-UA were calculated to discuss the O_3 spatial correlation. As displayed in Fig. 6a), from 2017 to 2020, the annual Moran's I was 1.63, 1.85, 1.63, and 2.09, respectively, and all the values passed the significance test. The positive annual Moran's I suggested the positive spatial autocorrelation and the spatial agglomeration of O_3 concentrations in the CP-UA. This indicated that O_3 in a city can be affected by its neighboring cities. In a previous study, it was found that O_3 concentrations were spatially agglomerated in BTH and PRD, but spatially dispersed in Chengdu-Chonqing [35]. The highest global Moran's I in CP-UA was found in summer (2.59), indicating a strengthening agglomerated distribution of O_3 concentrations. We inferred that the photochemical reactions were strong in summer which lead to the formation and accumulation of O_3. Hence, regional cooperation across cities is necessary. To identify the distribution and agglomeration patterns of O_3 pollution in each city of CP-UA, local spatial autocorrelation analysis was employed in this study. As shown in Fig. 6b), the most polluted cities were distributed in northern CP-UA, forming a high-high (HH) agglomeration of O_3 concentration. The HH agglomeration cities including Xingtai, Handan, Changzhi, Liaocheng, Anyang, Jiaozuo, and Xinxiang are mostly industrial cities with intensive anthropogenic emissions and insufficient precipitation. Cities in southern CP-UA had low O_3 concentrations, forming a low-low (LL) agglomeration (Fig. 6b). The LL agglomeration cities included Zhoukou, Zhumadian, Xinyang, Fuyang, Bengbu, and Bozhou. Those cities are all located in the south of the North-South climatic transition zone, which means abundant precipitation. To sum up, O_3 control by any individual city was insufficient, and joint efforts across the CP-UA would be necessary to reduce regional O_3 pollution. More stringent measures should be taken in the northern CP-UA.

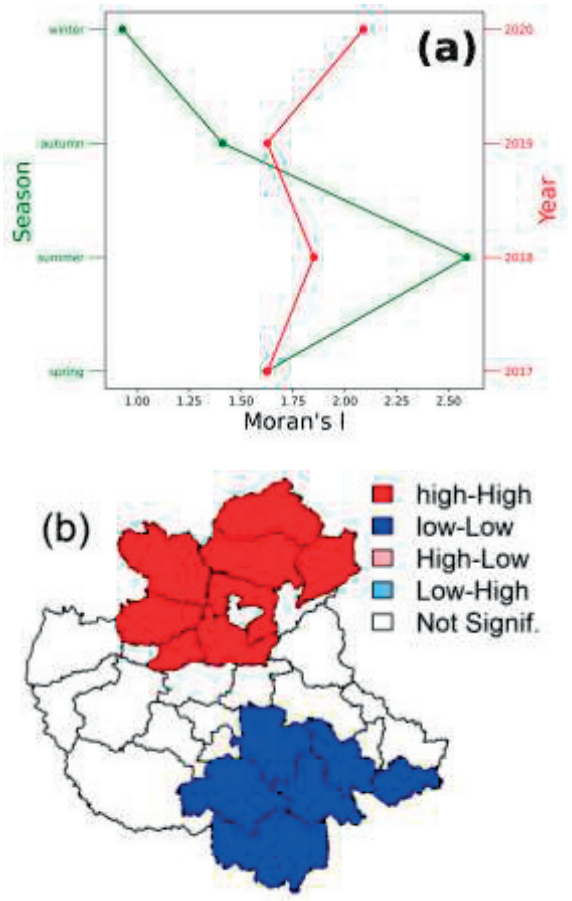

Fig. 6. a) Global Moran's I index and b) spatial agglomeration of O_3 concentrations in the CP-UA in 2017-2020.

Human Health Impacts

To estimate O_3 impacts on health in the CP-UA, the premature mortality attributed to O_3 in warm months (from April to September) was calculated. As displayed in Fig. 7, from 2017 to 2020, the premature mortality related to O_3 for respiratory disease in the CP-UA was 17438, 17087, 16765, and 12549, respectively, which was

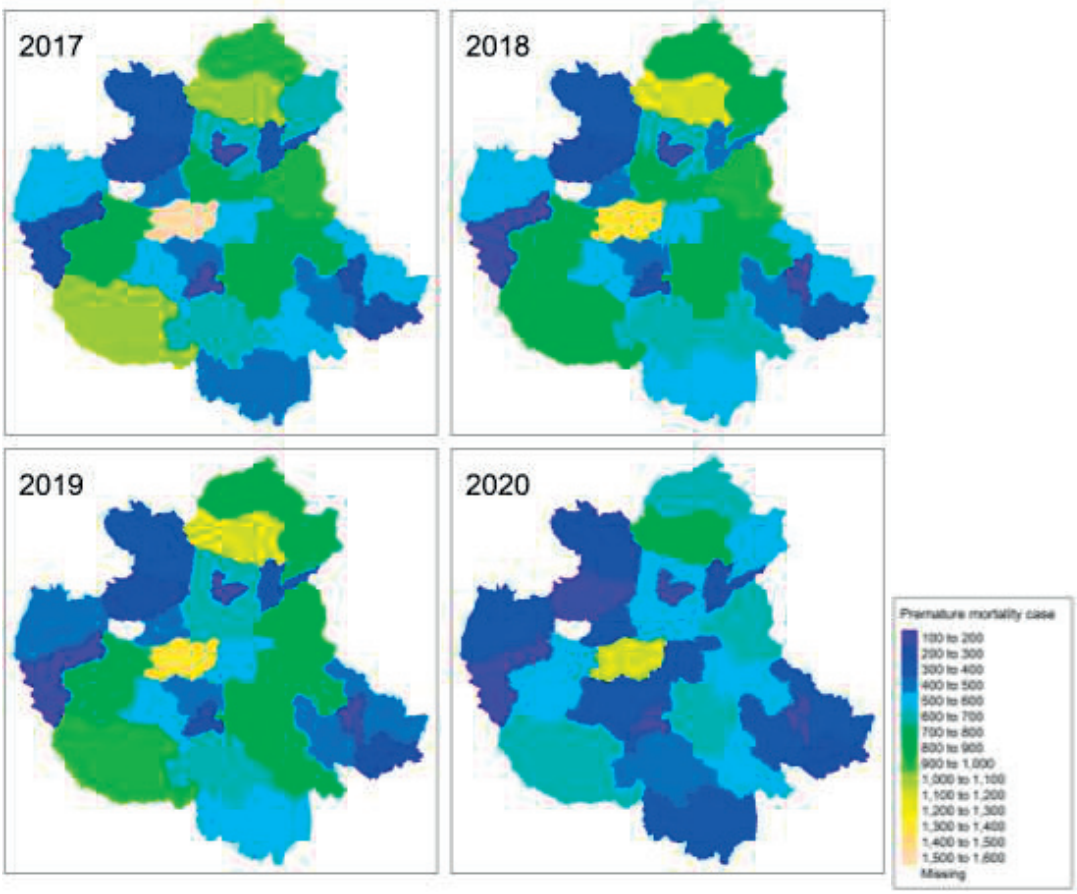

Fig. 7. The distribution of premature mortality attributed to O_3 exposure for respiratory disease in warm seasons (from April to September) in the CP-UA.

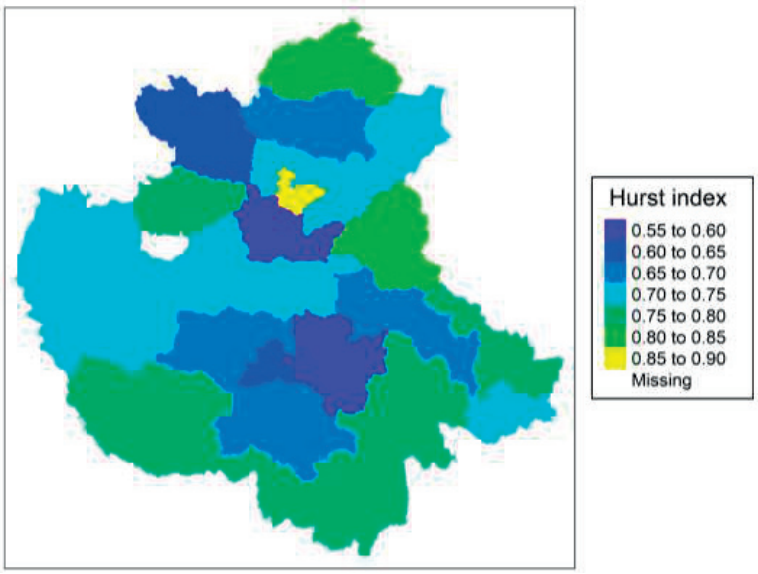

Fig. 8. Hurst index of O_3 concentration in the CP-UA.

much higher than in the YRD (5889 per year from 2015 to 2019) [34]. The reduction of premature mortalities in the CP-UA indicated that the measures taken by the Chinese government to control O_3 pollution have achieved good results. Among the 30 cities in the CP-UA, Zhengzhou was estimated to have the highest premature mortalities, with 1556, 1382, 1387, and 1110 cases in 2017, 2018, 2019, and 2020, respectively. Zhengzhou is the central city of the CP-UA, with a population of 12.6 million. The top ten cities with mean premature mortality from 2017 to 2020 related to O_3 were Zhengzhou (1358), Handan (1035), Nanyang (868), Heze (854), Xingtai (819), Zhoukou (816), Luoyang (718), Xinxiang (668), Shangqiu (693), and Anyang (613), respectively. In contrast, the city with the lowest premature deaths was Hebi due to its small population (1.566 million) and low O_3 concentration (147 μg/m^3 for a four-year average), with 191, 184, 174, and 137 cases in 2017, 2018, 2019, and 2020, respectively. We found that the population in some cities varies little, while the estimated premature mortalities vary largely. For example, the population of Xinxiang and Xinyang were 6251929 and 6234401, respectively, and the premature mortalities were 668 and 480, respectively. This suggested that premature mortality is sensitive to O_3 concentration. As can be seen from Equation 16, premature mortality increase with O_3 concentration exponentially.

The time-series domain rescaling analysis method was employed to calculate the Hurst index of O_3 concentration in the CP-UA. As displayed in Fig. 8, the Hurst index ranged from 0.59 to 0.85, all larger than 0.5, indicating the time series of O_3 was long-term persistent, that is, the change in O_3 concentration in the future is consistent with the changing trend in the past. As discussed in the previous section, the O_3 concentration in the CP-UA from 2017 to 2020 was gradually reduced. This suggested that the O_3 concentration in the CP-UA will continue to decline in the future. Therefore, we inferred that the premature mortality attributed to O_3 in the CP-UA will continue to decline. Luoyang, Changzhi, Xinxiang, Liaocheng, and Hebi ranked in the top 5 in terms of the Hurst index, which indicated that these cities are more likely to have a decline in O_3 concentration and premature mortality.

Conclusion

In this study, multiple transdisciplinary methods, including geographical analysis and spatial statistics, were used to investigate the spatiotemporal distribution variations and the human health impacts of O_3 in the CP-UA. The results of the study showed that the annual average concentration of O_3 in the CP-UA reduced by 19.7% in 2020, as compared to 2017. While, the proportion of MAD8-O_3 that exceeded the Grade 2 limit in 2020 was 29.3%, indicating still serious O_3 pollution. O_3 concentrations showed a multimodal structure trend with the month in the CP-UA, with the highest concentrations in June (195.5 μg/m^3). The O_3 concentrations showed a feature of "high in summer and winter, low in spring and autumn" in CP-UA. In diurnal changes, O_3 concentrations exhibited a unimodal trend, with high in the daytime and low in the nighttime. Concerning spatial distribution, the main distribution of O_3 concentration was aligned in the northwest-southeast direction for the CP-UA. From 2017 to 2020, the centers of O_3 concentrations across the CP-UA moved southeast. In summer and winter, the mean centers were located in Zhengzhou, and in spring and winter the mean centers moved to Kaifeng. O_3 concentrations exhibited positive spatial autocorrelations in the CP-UA. The spatial autocorrelation was strongest in summer. The most polluted cities were distributed in northern CP-UA, including Xingtai, Handan, Changzhi, Liaocheng, Anyang, Jiaozuo, and Xinxiang, forming a high-high (HH) agglomeration of O_3 concentration. Cities in southern CP-UA including Zhoukou, Zhumadian, Xinyang, Fuyang, Bengbu, and Bozhou, had low O_3 concentrations, forming a low-low (LL) agglomeration. According to our estimates, the premature mortality attributed to O_3 for respiratory disease in warm months was 15960 per year. The premature mortalities decreased by 28.7% in 2020 compared to 2017. Furthermore, the changing trend of O_3 concentration was predicted by rescaled range analysis. The calculated Hurst index of O_3 concentrations in all cities in the CP-UA was all larger than 0.5, indicating the declining trend of O_3 concentrations and premature mortalities in the CP-UA.

Acknowledgments

This work was Supported by National Natural Science Foundation of China (Grant No. 41771438), and the Program for Innovative Research Team (in Science and Technology) in University of Henan Province (Grant No. 22IRTSTHN010).

Conflicts of Interest

The authors declare no conflict of interest.

References

1. LIU H., LIU J., LIU Y., YI K., YANG H., XIANG S., MA J., TAO S. Spatiotemporal variability and driving factors of ground-level summertime ozone pollution over eastern China. Atmospheric Environment, **265**, 118686, **2021**.
2. GONG X., HONG S., JAFFE D.A. Ozone in China: Spatial Distribution and Leading Meteorological Factors Controlling O_3 in 16 Chinese Cities. Aerosol and Air Quality Research, **18** (9), 2287, **2018**.
3. WANG T., XUE L., BRIMBLECOMBE P., LAM Y.F., LI L., ZHANG L. Ozone pollution in China: A review

of concentrations, meteorological influences, chemical precursors, and effects. Science of The Total Environment, **575**, 1582, **2017**.
4. CHENG M., FANG F., NAVON I.M., ZHENG J., TANG X., ZHU J., PAIN C. Spatio-temporal hourly and daily ozone forecasting in China using a Hybrid machine learning model: Autoencoder and Generative Adversarial Networks. Journal of Advances in Modeling Earth Systems, **14** (3), e2021MS002806, **2022**.
5. ABDULLAH A.M., ISMAIL M., YUEN F.S., ABDULLAH S., ELHADI R. The relationship between daily maximum temperature and daily maximum ground level ozone concentration. Polish Journal of Environmental Studies, **26** (2), 517, **2017**.
6. WANG P., WANG P., CHEN K., DU J., ZHANG H. Ground-level ozone simulation using ensemble WRF/Chem predictions over the Southeast United States. Chemosphere, **287**, 132428, **2022**.
7. WANG Y., WILD O., ASHWORTH K., CHEN X., WU Q., QI Y., WANG Z. Reductions in crop yields across China from elevated ozone. Environmental Pollution, **292**, 118218, **2022**.
8. WANG Z., LV J., TAN Y., GUO M., GU Y., XU S., ZHOU Y. Temporospatial variations and Spearman correlation analysis of ozone concentrations to nitrogen dioxide, sulfur dioxide, particulate matters and carbon monoxide in ambient air, China. Atmospheric Pollution Research, **10** (4), 1203, **2019**.
9. ZHANG Y., MA Y., FENG F., CHENG B., SHEN J., WANG H., JIAO H., LI M. Respiratory mortality associated with ozone in China: A systematic review and meta-analysis. Environmental Pollution, **280**, 116957, **2021**.
10. ZHANG Z., YAO M., WU W., ZHAO X., ZHANG J. Spatiotemporal assessment of health burden and economic losses attributable to short-term exposure to ground-level ozone during 2015-2018 in China. BMC Public Health, **21** (1), 1069, **2021**.
11. MOUSAVINEZHAD S., CHOI Y., POUYAEI A., GHAHREMANLOO M., NELSON D.L. A comprehensive investigation of surface ozone pollution in China, 2015-2019: Separating the contributions from meteorology and precursor emissions. Atmospheric Research, **257**, 105599, **2021**.
12. TONG L., XIAO H., YI H., LIU Y., ZHENG J., HUANG C., HE M. Spatial regionalization on surface ozone in the Yangtze River Delta of China. Asia-Pacific Journal of Atmospheric Sciences, **58** (2), 207, **2022**.
13. ZHANG A., LIN J., CHEN W., LIN M., LEI C. Spatial-temporal distribution variation of ground-level ozone in China's Pearl River Delta metropolitan region. International Journal of Environmental Research and Public Health, **18** (3), 872, **2021**.
14. TANG K., ZHANG H., FENG W., LIAO H., HU J., LI N. Increasing but variable trend of surface ozone in the Yangtze River Delta Region of China. Frontiers in Environmental Science, **10**, 10, **2022**.
15. LIA Y., CHENG M., GUO Z., ZHANG X., CUI X., CHEN S. Increase in surface ozone over Beijing-Tianjin-Hebei and the surrounding areas of China inferred from satellite retrievals, 2005-2018. Aerosol and Air Quality Research, **20** (10), 2170, **2020**.
16. LU H., LYU X., CHENG H., LING Z., GUO H. Overview on the spatial-temporal characteristics of the ozone formation regime in China. Environmental Science: Processes & Impacts, **21** (6), 916, **2019**.
17. SHEN Y., ZHANG L., FANG X., JI H., LI X., ZHAO Z. Spatiotemporal patterns of recent $PM_{2.5}$ concentrations over typical urban agglomerations in China. Science of The Total Environment, **655**, 13, **2019**.
18. TAO T., SHI Y., GILBERT K.M., LIU X. Spatiotemporal variations of air pollutants based on ground observation and emission sources over 19 Chinese urban agglomerations during 2015-2019. Scientific Reports, **12** (1), 4293, **2022**.
19. LI Y., YIN S., YU S., BAI L., WANG X., LU X., MA S. Characteristics of ozone pollution and the sensitivity to precursors during early summer in central plain, China. Journal of Environmental Sciences, **99**, 354, **2021**.
20. YU S., SU F., YIN S., WANG S., XU R., HE B., FAN X., YUAN M., ZHANG R. Characterization of ambient volatile organic compounds, source apportionment, and the ozone–NO_x–VOC sensitivities in a heavily polluted megacity of central China: effect of sporting events and emission reductions. Atmospheric Chemistry and Physics, **21** (19), 15239, **2021**.
21. QIN L., GU J., LIANG S., FANG F., BAI W., LIU X., ZHAO T., WALLINE J., ZHANG S., CUI Y., XU Y., LIN H. Seasonal association between ambient ozone and mortality in Zhengzhou, China. International Journal of Biometeorology, **61** (6), 1003, **2017**.
22. WANG T., ZHANG L., ZHOU S., ZHANG T., ZHAI S., YANG Z., WANG D., SONG H. Effects of ground-level ozone pollution on yield and economic losses of winter wheat in Henan, China. Atmospheric Environment, **262**, 118654, **2021**.
23. LIN Y., JIANG F., ZHAO J., ZHU G., HE X., MA X., LI S., SABEL C., WANG H. Impacts of O_3 on premature mortality and crop yield loss across China. Atmospheric Environment, **194**, 41, **2018**.
24. FU X., LI L., LEI Y., WU S., YAN D., LUO X., LUO H. The economic loss of health effect damages from $PM_{2.5}$ pollution in the Central Plains Urban Agglomeration. Environmental Science and Pollution Research, **27** (20), 25434, **2020**.
25. YANG G., LIU Y., LI X. Spatiotemporal distribution of ground-level ozone in China at a city level. Scientific Reports, **10** (1), 7229, **2020**.
26. JIANG L., HE S., ZHOU H. Spatio-temporal characteristics and convergence trends of $PM_{2.5}$ pollution: A case study of cities of air pollution transmission channel in Beijing-Tianjin-Hebei region, China. Journal of Cleaner Production, **256**, 120631, **2020**.
27. SHI Y., MATSUNAGA T., YAMAGUCHI Y., ZHAO A., LI Z., GU X. Long-term trends and spatial patterns of $PM_{2.5}$ induced premature mortality in South and Southeast Asia from 1999 to 2014. Science of The Total Environment, **631**, 1504, **2018**.
28. WACHOWICZ M., LIU T. Finding spatial outliers in collective mobility patterns coupled with social ties. International Journal of Geographical Information Science, **30** (9), 1806, **2016**.
29. HURST H.E. Long-term storage capacity of reservoirs. Transactions of the American Society of Civil Engineers, **116**, 770, **1951**.
30. LIU X., HADIATULLAH H., TAI P., XU Y., ZHANG X., SCHNELLE-KREIS J., SCHLOTERHAI B., ZIMMERMANN R. Air pollution in Germany: Spatio-temporal variations and their driving factors based on continuous data from 2008 to 2018. Environmental Pollution, **276**, 116732, **2021**.
31. SUN Z.Q., SUN T. The Impact of Multi-Dimensional Urbanization on China's Carbon Emissions Based

on the Spatial Spillover Effect. Polish Journal of Environmental Studies, **29** (5), 3317, **2020**.
32. TANG D., XU H., YANG Y. Mutual Influence of Energy Consumption and Foreign Direct Investment on Haze Pollution in China: a Spatial Econometric Approach. Polish Journal of Environmental Studies, **27** (4), 1743, **2018**.
33. SU Y., LU C., LIN X., ZHONG L., GAO Y., LEI Y. Analysis of spatio-temporal characteristics and driving forces of air quality in the northern coastal comprehensive economic zone, China. Sustainability, **12** (2), 536, **2020**.
34. ZHAN C., XIE M., LIU J., WANG T., XU M., CHEN B., LI S., ZHUANG B., LI M. Surface ozone in the Yangtze River Delta, China: A synthesis of basic features, meteorological driving factors, and health impacts. Journal of Geophysical Research: Atmospheres, **126** (6), e2020JD033600, **2021**.
35. LIU X., ZHAO C., NIU J., SU F., YAO D., XU F., YAN J., SHEN X., JIN T. Spatiotemporal patterns and regional transport of ground-level ozone in major urban agglomerations in China. Atmosphere, **13** (2), 301, **2022**.
36. YIN C.Q., SOLMON F., DENG X.J., ZOU Y., DENG T., WANG N., LI F., MAI B., LIU L. Geographical distribution of ozone seasonality over China. Science of The Total Environment, **689**, 625, **2019**.
37. ZHU Q., BI J., LIU X., LI S., WANG W., ZHAO Y., LIU Y. Satellite-based long-term spatiotemporal patterns of surface ozone concentrations in China: 2005-2019. Environmental Health Perspectives, **130** (2), 27004, **2022**.
38. LIANG L., WANG Z. Control models and spatiotemporal characteristics of air pollution in the rapidly developing urban agglomerations. International Journal of Environmental Research and Public Health, **18** (11), 6177, **2021**.
39. LI K., JACOB D.J., LIAO H., QIU Y., SHEN L., ZHAI S., BATES K., SULPRIZIO M., SONG S., LU X., ZHANG Q., ZHENG B., ZHANG Y., ZHANG J., LEE H., KUK S.K. Ozone pollution in the North China Plain spreading into the late-winter haze season. Proceedings of the National Academy of Sciences, **118** (10), **2021**.
40. XIA N., DU E., GUO Z., DE VRIES W. The diurnal cycle of summer tropospheric ozone concentrations across Chinese cities: Spatial patterns and main drivers. Environmental Pollution, **286**, 117547, **2021**.
41. COYLE M., SMITH R.I., STEDMAN J.R., WESTON K.J., FOWLER D. Quantifying the spatial distribution of surface ozone concentration in the UK. Atmospheric Environment, **36** (6), 1013, **2002**.
42. LI K., JACOB D.J., LIAO H., ZHU J., SHAH V., SHEN L., BATES K., ZHANG Q., ZHAI S. A two-pollutant strategy for improving ozone and particulate air quality in China. Nature Geoscience, **12** (11), 906, **2019**.